AGU PUBLICATIONS

Geophysical Research Letters

RESEARCH LETTER
10.1002/2016GL070526

Key Points:
- A negative AO response appears in winter with more heat transport into the Arctic in either case of realistic or extreme Arctic sea ice loss
- Arctic sea ice impacts midlatitude climate via two pathways: the stratospheric and tropospheric pathways

Supporting Information:
- Supporting Information S1

Correspondence to:
T. Nakamura,
nakamura.tetsu@ees.hokudai.ac.jp

Citation:
Nakamura, T., K. Yamazaki, M. Honda, J. Ukita, R. Jaiser, D. Handorf, and K. Dethloff (2016), On the atmospheric response experiment to a Blue Arctic Ocean, *Geophys. Res. Lett.*, *43*, 10,394–10,402, doi:10.1002/2016GL070526.

Received 18 MAY 2016
Accepted 7 SEP 2016
Accepted article online 10 SEP 2016
Published online 6 OCT 2016

On the atmospheric response experiment to a Blue Arctic Ocean

Tetsu Nakamura[1,2], Koji Yamazaki[1,2], Meiji Honda[3], Jinro Ukita[3], Ralf Jaiser[4], Dörthe Handorf[4], and Klaus Dethloff[4]

[1]Faculty of Environmental Earth Science, Hokkaido University, Sapporo, Japan, [2]Arctic Environmental Research Center, National Institute of Polar Research, Tokyo, Japan, [3]Faculty of Science, Niigata University, Niigata, Japan, [4]Helmholtz-Zentrum für Polar- und Meeresforschung, Alfred-Wegener-Institut, Potsdam, Germany

Abstract We demonstrated atmospheric responses to a reduction in Arctic sea ice via simulations in which Arctic sea ice decreased stepwise from the present-day range to an ice-free range. In all cases, the tropospheric response exhibited a negative Arctic Oscillation (AO)-like pattern. An intensification of the climatological planetary-scale wave due to the present-day sea ice reduction on the Atlantic side of the Arctic Ocean induced stratospheric polar vortex weakening and the subsequent negative AO. Conversely, strong Arctic warming due to ice-free conditions across the entire Arctic Ocean induced a weakening of the tropospheric westerlies corresponding to a negative AO without troposphere-stratosphere coupling, for which the planetary-scale wave response to a surface heat source extending to the Pacific side of the Arctic Ocean was responsible. Because the resultant negative AO-like response was accompanied by secondary circulation in the meridional plane, atmospheric heat transport into the Arctic increased, accelerating the Arctic amplification.

1. Introduction

Arctic warming is among the most remarkable of climate change signals undergoing global warming and has resulted in continuous changes to the Arctic environment. Arctic sea ice loss is one of the most symbolic signatures of these rapid climate changes. Changes to Arctic sea ice are crucial to the coupled climate system, because ice melting is stimulated by atmospheric and oceanic heat transport into the Arctic. In turn, radiative and thermal feedback from the melting ice induces further warming in the Arctic. In this context, there is particular interest in the recent negative tendency of the winter Arctic Oscillation (AO) [*Thompson and Wallace*, 1998, 2001] observed in association with the loss of Arctic sea ice [*Honda et al*., 2009; *Jaiser et al*., 2012; *Liu et al*., 2012] and an increase in the extent of Eurasian snow cover [*Cohen et al*., 2014; *Furtado et al*., 2016]. The negative phase of the AO is a manifestation of the exchange of the Arctic cold air mass and midlatitude warm air mass following a stronger meandering of the flow, which implies an increase in atmospheric heat transport into the Arctic. Such circulation changes associated with a negative AO enhance Arctic warming and local surface heat flux anomalies due to Arctic sea ice loss.

Observational [*King et al*., 2015; *Jaiser et al*., 2016; *Yang et al*., 2016] and modeling [*Kim et al*., 2014; *Nakamura et al*., 2015, 2016; *Wu and Smith*, 2016] studies have demonstrated possible impacts of sea ice reduction on stratospheric polar vortex weakening, which is often accompanied by a negative AO in the troposphere through downward control via wave-mean flow interaction processes [*Haynes et al*., 1991; *Baldwin and Dunkerton*, 2001; *Kidston et al*., 2015]. This is likely caused by interferences between climatological and anomalous planetary-scale wave structures [*Sun et al*., 2015]. Despite intensive efforts, the association between the AO and Arctic sea ice changes remains unclear. In particular, the impacts of sea ice loss on severe cold winters in the midlatitudes, a typical characteristic of the negative AO, are not always reproduced in different model simulations [*Screen and Simmonds*, 2013; *Screen et al*., 2013]. This is partly due to differences in experimental design or boundary conditions. In addition, large and chaotic atmospheric internal variability and warming due to other climate forcing factors often mask signals from the impacts of sea ice [*Mori et al*., 2014; *Deser et al*., 2016]. Nonlinear behavior in the sea ice-AO relationship has been discussed [*Petoukhov and Semenov*, 2010], as well as the impact of the Arctic on midlatitude climate under future warming climate conditions [*Sun et al*., 2015; *Wu and Smith*, 2016].

In this study, we examined how the impacts of climate on Arctic sea ice changes are modified during the transition from present-day conditions to ice-free conditions. We conducted four sensitivity experiments

Table 1. Outline of the Experimental Setup[a]

Run	Integration Period (Years)	SST	SIT
CNTL	150	*Climatology*	*High* ice period, 1979–1983
AICE	150	*Climatology*	*Low* ice period, 2005–2009
Im30	150	*Climatology*	Decrease of 30 cm from *CNTL*
Im40	150	*Climatology*	Decrease of 40 cm from *CNTL*
Im50	150	*Climatology*	Decrease of 50 cm from *CNTL*

[a]*Climatology* is the time period of 1981–2010 for which the monthly average sea surface temperature (SST) was used for the boundary conditions. *High* (1979–1983) and *low* (2005–2009) years are the time periods for which the monthly average sea ice thickness (SIT) was used for the boundary conditions.

using the idealized assumption that Arctic sea ice is reduced to the ice-free condition in a stepwise manner. Then, we adopted an atmospheric general circulation model (AGCM) that has successfully captured the negative AO-like responses to a reduction in sea ice [*Nakamura et al*., 2015, 2016; *Jaiser et al*., 2016]. Our comparison of the atmospheric responses to gradual changes in sea ice improves our understanding of the underlying mechanism of the association between sea ice and the AO.

2. Methods

2.1. Model and Experimental Design

We used the same model and observational data for the boundary conditions as that in our previous study [*Nakamura et al*., 2016] using the AGCM for the Earth Simulator (AFES) version 4.1, with triangular truncation at horizontal wave number 79 (T79; horizontal resolution: ~1.5°), 56 vertical levels, a model top of ~60 km, and Merged Hadley–National Oceanic and Atmospheric Administration (NOAA)/Optimum Interpolation Sea Surface Temperature (SST) and Sea Ice Concentration (SIC) data sets [*Hurrell et al*., 2008]. To demonstrate the impact of reductions in present-day sea ice, we defined *high* (5 year average of 1979–1983) and *low* (2005–2009) periods. Corresponding to changes in sea ice coverage (*low* minus *high*), obvious sea ice loss was found in the Pacific side of the Arctic Ocean in summer and in the Atlantic side in winter (see Figure S1 in the supporting information). In our previous paper [*Nakamura et al*., 2015], we addressed our treatment of sea ice, which is relevant to quantifying sea ice in the perturbed runs in this study: "Our model does not treat SIC directly; instead, each model grid cell is either treated as being ice covered or ice free. We assumed a maximum sea ice thickness (SIT) in the Arctic of 50 cm, so that SIC from 0 to 100% was linearly converted into SIT from 0 to 50 cm. We then set all grid cells where converted SIT was less than 5 cm to 0 cm (i.e., no ice). By this procedure, the simulated heat flux in the Arctic of our model is comparable with observations." Note that the SIC-to-SIT conversion does not consider the fractional surface roughness parameter. The roughness of ice is a constant value that does not depend on thickness. This could result in an overestimation of the near-surface temperature over the sea ice grid, although only within several kelvin at the most.

We performed 150 year integrations of a control run (*CNTL*) and four perturbed runs, referred to as *AICE*, *Im30*, *Im40*, and *Im50*, in which the sea ice conditions were varied as summarized in Table 1 (also see section S1 in the supporting information). While the climatological SST and sea ice conditions of the *high* period were used in *CNTL*, the sea ice condition of the *low* period was used in an anomalous ice (*AICE*) run. Alternative low sea ice conditions were used in *Im30* and *Im40* runs, in which SITs were artificially and impartially reduced by 30 and 40 cm from the *high* condition in all grids over the Arctic Ocean. In the *Im50* run, SIT was reduced by 50 cm, indicating an ice-free condition over the Arctic Ocean in all seasons (see section S1). We emphasize that this experimental setup, without any changes to external conditions other than sea ice, was designed in an attempt to better understand the physical processes underlying the association between sea ice and the AO. In reality, sea ice will retreat more intensively over the marginal regions and much more weakly over the central Arctic. Therefore, runs with intermediate sea ice loss (i.e., *Im30* and *Im40*) are not necessarily representative of the actual transition from the present-day condition to an ice-free condition.

2.2. Statistics and Techniques

We examined the differences in the 150 year averages of the respective perturbed runs against the *CNTL* run with a Student's two-sided *t* test. The vertical component of the Eliassen-Palm (E-P) flux (*Fz*) obtained from transformed Eulerian mean (TEM) diagnostics of the daily mean field was used as an indicator of upward

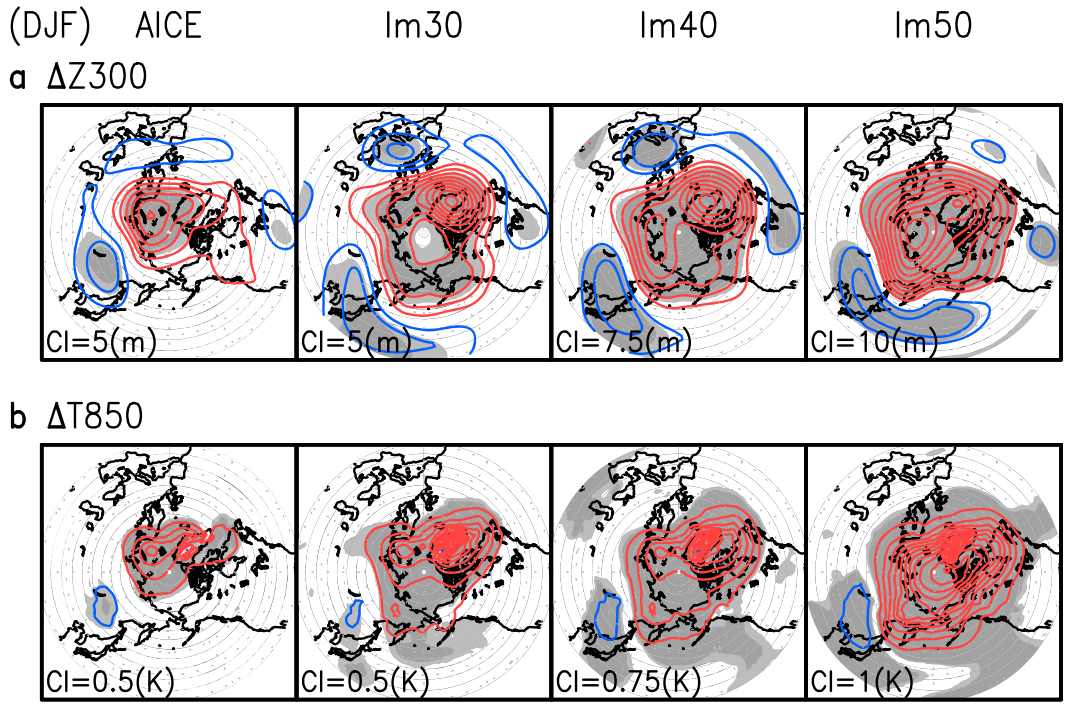

Figure 1. Differences in the 150 year average of the (a) geopotential height at 300 hPa (m) and (b) temperature at 850 hPa (K) in December-January-February. Anomalies of (from left to right) *AICE*, *Im30*, *Im40*, and *Im50* runs from the *CNTL* run are shown. A positive (negative) anomaly is indicated by red (blue) contours. The zero line is omitted and the contour interval is displayed at the bottom left corner of the plot. Statistical significance greater than 95% and 99% are indicated by light and heavy gray shading, respectively. *CNTL*, *high* ice period, 1979–1983; *AICE*, *low* ice period, 2005–2009; *Im30*, *Im40*, and *Im50*: decrease of 30, 40, and 50 cm, respectively, from the *CNTL*.

propagating planetary wave activity. An 11 day boxcar filter was applied to zonal mean zonal wind and *Fz* before analyzing the daily evolutions. A Fourier transformation was applied to the atmospheric field to decompose the wave number component and diagnose atmospheric changes by separating them into planetary and synoptic scales. We defined the planetary-scale wave and the synoptic-scale wave as waves 1 plus 2 (wave1 + 2) and waves 3 to 10 (wave3–10), respectively. The atmospheric heating rate due to the anomalous residual mean vertical motion (w^*) was estimated from TEM diagnosis (see section S2) and compared to the direct turbulent heat flux anomaly due to Arctic sea ice changes.

3. Results and Discussion

3.1. Responses of the Tropospheric Circulation

The winter Northern Hemisphere (NH) atmospheric response to a reduction in present-day sea ice clearly showed a negative AO-like pattern in the upper tropospheric height anomaly (ΔZ300; Figure 1a, *AICE*). The corresponding near-surface temperature response (ΔT850) was indicative of a warm anomaly over the Atlantic side of the Arctic Ocean, due to the reduction in sea ice in that area, and a cold anomaly over eastern Siberia (Figure 1b, *AICE*).

Even when SIT was further reduced artificially as described above, the tropospheric responses showed negative AO-like patterns with amplitudes that increased as more sea ice was reduced (Figure 1a, *Im30* and *Im40*). Under ice-free conditions, the atmospheric response maintained a negative AO-like pattern with the maximum amplitude (Figure 1a, *Im50*). In addition, lower tropospheric air temperature responses maintained a warm Arctic and cold Siberian pattern, with amplified warm anomalies over the Pacific side of the Arctic Ocean in association with the large reductions in sea ice in the respective cases (Figure 1b, *Im30*, *Im40*, and *Im50*).

Our experiments showed that the negative AO-like pattern intensifies with a reduction in Arctic sea ice. This appears to be consistent with current studies that presented a negative phase shift of the AO induced by the

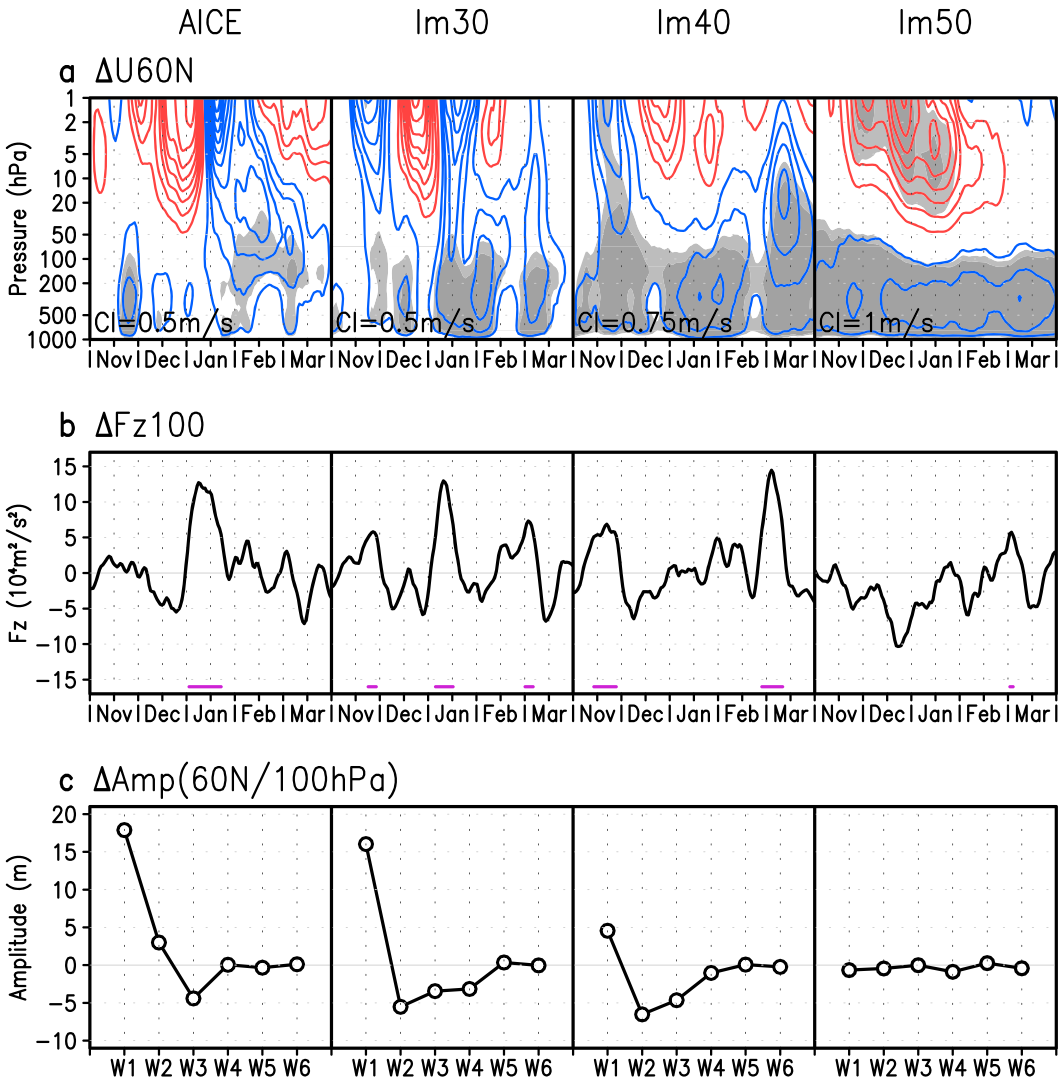

Figure 2. (a) Daily evolutions of zonal mean zonal wind anomalies (respective runs minus *CNTL*) at 60°N. The contours and shading are the same as those in Figure 1. (b) Daily evolutions of *Fz* (i.e., vertical component of the Eliassen-Palm (E-P) flux) anomalies at 50–80°N and 100 hPa. Periods when the *Fz* anomaly exceeded 5×10^4 m^2 s^{-2} are indicated by a purple line. (c) Anomalies of amplitude (i.e., square root of the power) decomposed into wave 1 to wave 6 components of January geopotential height at 60°N and 100 hPa.

recent Arctic sea ice reduction [*Jaiser et al.*, 2012; *Liu et al.*, 2012; *Nakamura et al.*, 2015]. Some studies have emphasized the role of stratosphere-troposphere coupling on the association between sea ice and the AO [*Kim et al.*, 2014; *King et al.*, 2015; *Jaiser et al.*, 2016; *Nakamura et al.*, 2016]. However, stratospheric responses vary depending on the location of sea ice anomalies [*Sun et al.*, 2015]. Therefore, we clarified the role of the stratosphere in our experiments.

3.2. Stratosphere-Troposphere Coupling Process

The daily evolution of the zonal mean zonal wind response at 60°N (ΔU60N) showed a relatively weak and continuous negative anomaly of about -0.5 m s^{-1} from November to March over the entire troposphere in *AICE* (Figure 2a). The tropospheric negative anomaly of the zonal wind corresponded to the negative phase of the AO, consistent with the height patterns shown in Figure 1a. Unlike the troposphere, a negative wind anomaly over -4.0 m s^{-1} appeared suddenly in the upper stratosphere in mid-January, indicative of a weakening of the polar vortex. This propagated downward, connecting with the tropospheric signal from January to March. The stratospheric wind anomaly followed an intensification of upward propagation of wave activity

in the lower stratosphere (ΔFz100), as indicated by a cluster of positive anomalies in early January (purple lines in Figure 2b, *AICE*).

The intensification of the upward wave propagation and subsequent stratospheric polar vortex weakening occurred sporadically in *Im30* and *Im40* (Figures 2a and 2b). Conversely, the negative tropospheric anomalies of the zonal wind were relatively large and significant, suggestive of independent tropospheric processes that differed from stratosphere-troposphere coupling. This independence between the stratosphere and troposphere was most obvious in *Im50* (Figure 2a), in which the stratospheric polar vortex strengthened from November to February, consistent with the reduced upward wave propagation (Figure 2b).

To examine why the intensity of the stratosphere-troposphere coupling weakened with increasing sea ice reduction, we applied a wave number analysis to the January mean height field in the lower stratosphere, an important level that connects the troposphere with the stratosphere through upward planetary-scale wave propagation [*Nakamura et al*., 2016]. We chose January due to the clear contrast between the *AICE* and *Im50* cases. The wave 1 amplitude of the 100 hPa geopotential height at 60°N was magnified clearly by 18 m (i.e., geopotential meter) in *AICE* (Figure 2c). While the wave 1 amplitudes were magnified by 16 and 5 m in *Im30* and *Im40*, respectively, no change was observed in *Im50*. This suggests that the wave 1 structure corresponding to a typical planetary-scale wave was responsible for the stratospheric polar vortex weakening. Therefore, we compared differences in the horizontal wave structure between the two most contrasting cases, *AICE* and *Im50*. The negative height anomaly appeared over eastern Siberia in both cases. However, in *Im50*, the positive height anomaly over the Arctic Ocean extended more than in *AICE* (Figure 1a, *AICE* and *Im50*). The lower stratospheric patterns and their wave 1 and wave 2 components were consistent with this feature (see section S3). The resultant height anomalies (ΔZ100) overlaid with the climatological Siberian trough, which has been discussed in conjunction with the stratospheric responses from the local interference between climatological and anomalous planetary-scale waves [*Sun et al*., 2015]. Therefore, we suggest that the intensification (suppression) of the climatological Siberian trough in the lower stratosphere could strengthen (weaken) stratosphere-troposphere coupling, which has a role in the association between sea ice and the AO in accordance with features of the recent Arctic amplification [*Cohen et al*., 2014].

3.3. Intensified Arctic Amplification via Atmospheric Heat Transport

Remaining interest is the tropospheric process governing the continuous negative AO-like response from November to March (Figure 2a, all cases) and its implication for Arctic amplification.

Using the TEM diagnosis, we examined the primary cause of the weakened circumpolar circulations corresponding to the negative AO in the troposphere from November to March. In all cases, negative anomalies of E-P flux divergence (i.e., decelerating zonal wind by wave forcing) appeared in the upper troposphere of the middle to high latitudes with magnitudes of -0.4 to $-1.2\,\mathrm{m\,s^{-1}\,d^{-1}}$ (Figure 3a). We decomposed this E-P flux divergence into meridional (i.e., eddy momentum flux) and vertical (i.e., eddy heat flux) components and into the planetary-scale (wave1 + 2) and synoptic-scale (wave3–10) waves. The vertical component of the wave forcing (*dFz*/*dz*), due to the planetary-scale wave (Pl), led to total deceleration (To) in all cases; the synoptic-scale wave (Sy) also contributed slightly (Figure 3b, red lines). This may be explained by the response of the stationary tropospheric Rossby wave to a reduction in Arctic sea ice [*Honda et al*., 2009; *Nakamura et al*., 2015]. The resulting increase in the meandering of the tropospheric jet stream induced a negative phase shift of the AO polarity (see section S4) [*Nakamura et al*., 2015]. While an intensification of the tropospheric planetary-scale wave does not necessarily connect with the lower stratosphere (see section S5), the resulting deceleration forcing in the upper troposphere may induce additional feedback via the meridional eddy momentum flux. The meridional component of the wave forcing (*dFy*/*dy*), in which contributions of planetary- and synoptic-scale waves are relatively comparable, also decelerated the zonal wind, but their amplitudes were relatively small (Figure 3b, green lines). This secondary deceleration due to the meridional component may result from the eddy response to the weakened westerly flow. The eddy feedback mechanism is a typical characteristic of the AO [*Limpasuvan and Hartmann*, 2000; *Kimoto et al*., 2001]. This is consistent with appearances of the negative AO-like response in all cases in this experiment. Note that there was a longitudinal dependency of the wave responses. While the tropospheric planetary-scale wave responses over eastern Siberia (e.g., Figure S4b) were only expected to decelerate the upper tropospheric jet stream above, the resultant total response in height showed a more annular structure

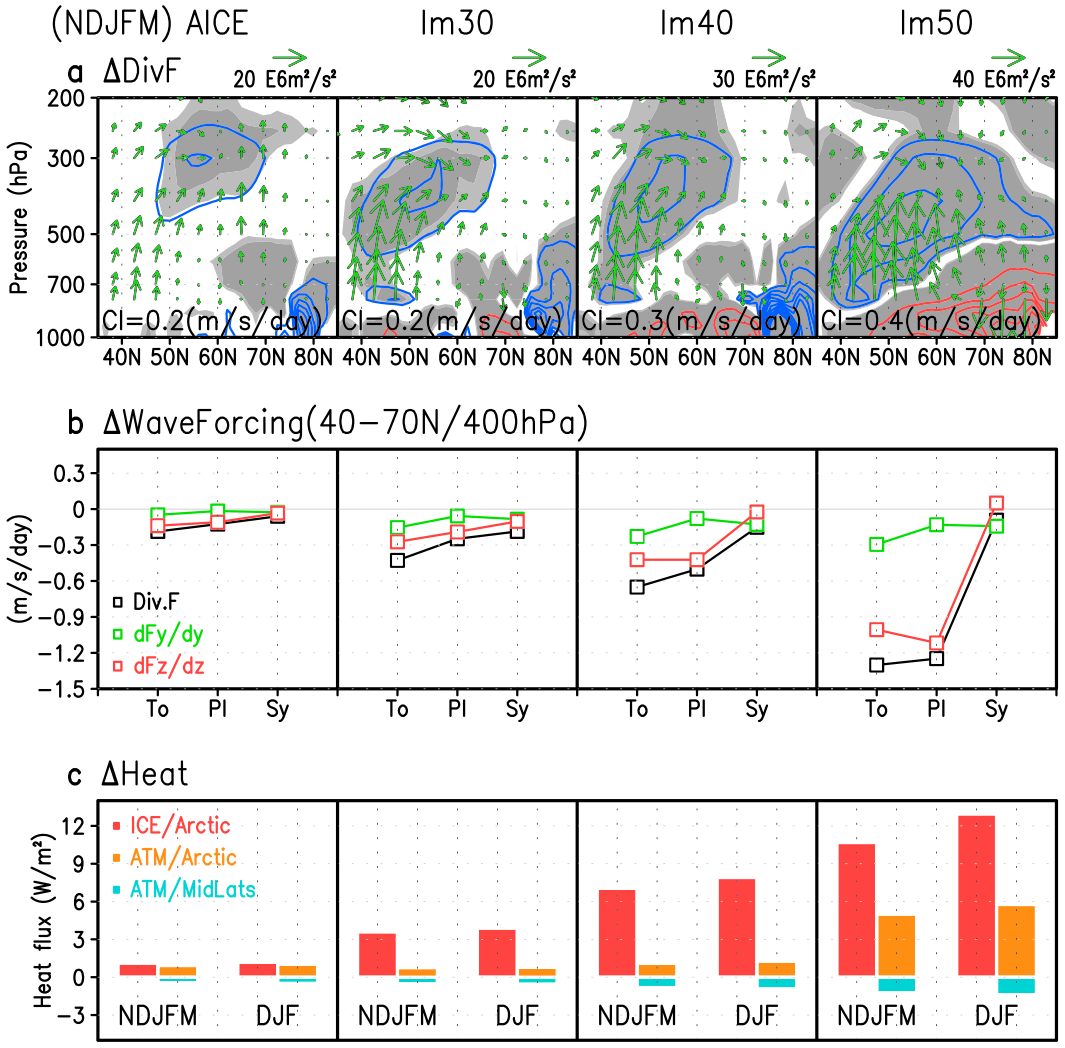

Figure 3. (a) November–March average anomalies of the E-P flux divergence ($m\,s^{-1}\,d^{-1}$) and corresponding E-P flux vectors (arrows). The contours and shading are the same as those in Figure 1, except that the contour interval of the positive anomaly is magnified by a factor of 10 to better visualize the contours near the surface where transformed Eulerian mean (TEM) diagnosis is not reliable. (b) November–March wave forcing anomalies due to a divergence of E-P flux (black), meridional E-P flux (green), and vertical E-P flux (red), averaged over 40–70°N at 400 hPa. To, Pl, and Sy in each plot indicate the total (all wave numbers), planetary-scale (wave1 + 2), and synoptic-scale (wave3–10) waves, respectively. (c) Anomalies of turbulent heat flux averaged poleward of 60°N (red), atmospheric heat transport averaged poleward of 60°N (orange), and atmospheric heat transport averaged over 30–60°N (cyan). The average anomalies from November to March (NDJFM) and December to February (DJF) are displayed on the left and right sides of the plot, respectively.

(i.e., AO like; see Figure 1a). This issue could not be addressed any more in the present study, although it may reflect the characteristics of the AO as a mode of NH atmospheric variability.

Considering the weakened meridional temperature gradient due to Arctic warming, the increase in tropospheric upward wave propagation was interesting because it induced anomalous atmospheric heat transport into the Arctic. This had the additional implication of inducing anomalous secondary circulations in the meridional plane via wave forcing. Deceleration forcing in the upper troposphere induced anomalous subsidence ($w^* < 0$) over the Arctic and anomalous upwelling ($w^* > 0$) over the midlatitude (see section S6), which was in agreement with the high- and low-pressure anomalies corresponding to the negative phase of the AO. This anomalous meridional circulation corresponded to anomalous heat transport into the Arctic. We estimated the atmospheric heat transport by this anomalous circulation and compared it with the vertical turbulent heat flux anomaly over the Arctic. In all cases, turbulent heat flux predominantly warmed the atmosphere

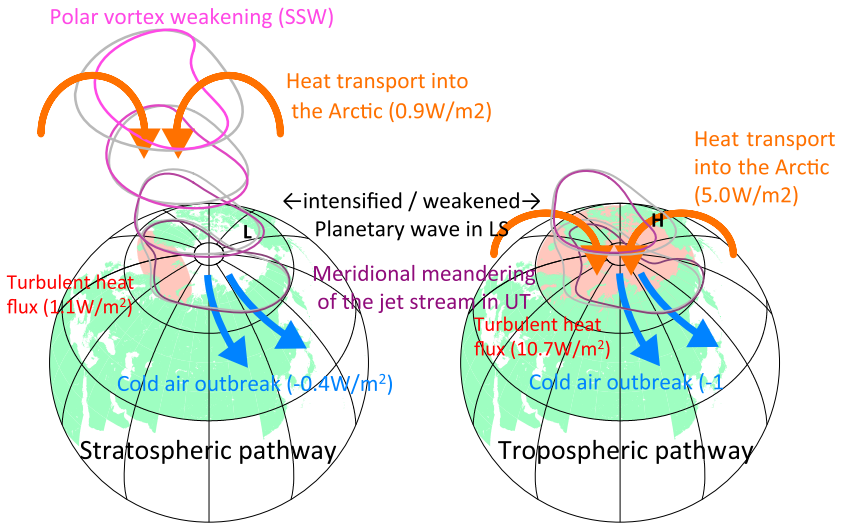

Figure 4. Schematic diagram of the two physical processes connecting Arctic sea ice loss and a negative Arctic Oscillation (AO)-like response. (left) The stratospheric pathway corresponding to the *AICE* case in January. (right) The tropospheric pathway corresponding to NDJFM *Im50* case. Typical characteristics of the circumpolar jet stream at 10, 30, 100, and 300 hPa (only 100 and 300 hPa in the right plot) corresponding to the *high* and *low* sea ice cases are shown by gray and purple lines, respectively. Anomalous atmospheric heating due to associated meridional circulation changes (see sections 3.3, S2, and S6) and the turbulent heat flux are given in units of W m^{-2}. SSW, sudden stratospheric warming; LS, lower stratosphere; UT, upper troposphere.

over the Arctic and the anomalous meridional circulation warmed the Arctic and cooled the midlatitudes (Figure 3c), although there were significant differences in amplitude among the cases. The results indicated that the anomalous meridional circulation, induced by the Arctic sea ice reduction, transported heat into the Arctic, in addition to the turbulent heat flux due to sea ice changes. This dynamic positive feedback could work independently of the stratospheric process, intensifying the Arctic amplification.

4. Concluding Remarks

We propose that there are two processes that control the association between Arctic sea ice changes and the polarity of the winter AO, which are described below.

1. The stratosphere-troposphere coupling process is dominated by an intensified climatological planetary-scale wave structure (Figure 4, the stratospheric pathway). This is mainly due to the intensification of the lower stratospheric Siberian trough associated with a reduction in Arctic sea ice on the Atlantic side of the Arctic Ocean. Our results are consistent with recent studies that demonstrated the role of the stratosphere in the association between sea ice and climate observed in the most recent decade [*Kim et al.*, 2014; *King et al.*, 2015; *Nakamura et al.*, 2016]. The results support that there are different stratospheric responses to different locations of surface heat sources [*Sun et al.*, 2015].
2. The tropospheric process is controlled by the eddy heat flux due to a planetary-scale wave response in the troposphere (Figure 4, the tropospheric pathway). Increased meandering of the tropospheric jet stream, corresponding to the response of the stationary Rossby wave to Arctic sea ice reduction [*Honda et al.*, 2009; *Nakamura et al.*, 2015], induces a negative AO-like pattern. Although the issue of longitudinal dependency remains, the associated eddy momentum flux response is consistent with the conventional understanding of AO dynamics [*Limpasuvan and Hartmann*, 2000; *Kimoto et al.*, 2001].

The experimental design of this study was highly idealized to isolate the impacts of sea ice and did not consider the direct impacts of SST or increasing greenhouse gases. However, the results provide an overview as to how the response of the NH climate to Arctic sea ice loss may be modified. Our results revealed two regimes. When Arctic sea ice loss retained the present-day geographic pattern, the lower stratospheric wave 1 structure, enhanced by the positive surface heat flux anomaly, became more concentrated on the Atlantic side of the Arctic Ocean, which perturbed the stratospheric polar vortex. In comparison, when the Arctic Ocean became ice free, the resulting surface heat flux anomalies over the entire Arctic weakened the

coupling between the troposphere and stratospheric polar vortex. Besides the different locations of the surface heat sources, the small-scale eddy and interaction with the planetary-scale eddy may be critical to determining the extent to which the troposphere is coupled to the stratosphere. For example, it has been suggested that the faster response of the baroclinic eddy to Arctic warming influences slower planetary-scale wave responses [*Semmler et al*., 2016]. This may be a key process in determining the polarity of the AO controlled by planetary-scale wave forcing.

Moreover, the results suggest a mechanism by which Arctic warming may interact with Arctic and midlatitude climate change. Additional dynamically induced heat transport into the Arctic occurred as a response to sea ice reduction, regardless of whether the stratospheric or tropospheric process was dominant. The initial reduction in sea ice due to Arctic warming strengthened dynamic heat transport and accelerated Arctic warming as positive feedback. While a relationship between Arctic warming and extreme weather in the midlatitude is still under debate [*Hassanzadeh et al*., 2014], the positive feedback of the Arctic warming associated with sea ice loss may yield unexpected severe hazards by amplifying the meandering of the tropospheric jet stream [*Francis and Vavrus*, 2012; *Screen and Simmonds*, 2014].

Acknowledgments

We thank the two anonymous reviewers for their constructive comments, which helped us to improve the manuscript. The Merged Hadley–NOAA/OI SST and SIC data were obtained from the Climate Data Guide (https://climatedataguide.ucar.edu/). The simulations were performed on the Earth Simulator at the Japan Agency for Marine-Earth Science and Technology. To access our simulation data, contact the corresponding author (nakamura.tetsu@ees.hokudai.ac.jp). The Green Network of Excellence Program Arctic Climate Change Research Project and the Arctic Challenge for Sustainability supported this study. The authors have no competing interests that might be perceived to influence the results and/or discussion reported in this article.

References

Baldwin, M. P., and T. J. Dunkerton (2001), Stratospheric harbingers of anomalous weather regimes, *Science*, *294*, 581–584.

Cohen, J., et al. (2014), Recent Arctic amplification and extreme mid-latitude weather, *Nat. Geosci.*, *7*, 627–637, doi:10.1038/NGEO2234.

Deser, C., L. Sun, R. A. Tomas, and J. Screen (2016), Does ocean coupling matter for the northern extratropical response to projected Arctic sea ice loss?, *Geophys. Res. Lett.*, *43*, 2149–2157, doi:10.1002/2016GL067792.

Francis, J. A., and S. J. Vavrus (2012), Evidence linking Arctic amplification to extreme weather in mid-latitude, *Geophys. Res. Lett.*, *39*, L06801, doi:10.1029/2012GL051000.

Furtado, J. C., J. L. Cohen, and E. Tziperman (2016), The combined influences of autumnal snow and sea ice on Northern Hemisphere winters, *Geophys. Res. Lett.*, *43*, 3478–3485, doi:10.1002/2016GL068108.

Hassanzadeh, P., Z. Kuang, and B. F. Farrell (2014), Responses of mid-latitude blocks and wave amplitude to changes in the meridional temperature gradient in an idealized dry GCM, *Geophys. Res. Lett.*, *41*, 5223–5232, doi:10.1029/2014GL060764.

Haynes, P. H., C. J. Marks, M. E. McIntyre, T. G. Shepherd, and K. P. Shine (1991), On the "downward control" of extratropical diabatic circulations by eddy-induced mean zonal forces, *J. Atmos. Sci.*, *48*, 651–678.

Honda, M., J. Inoue, and S. Yamane (2009), Influence of low Arctic sea-ice minima on anomalously cold Eurasian winters, *Geophys. Res. Lett.*, *36*, L08707, doi:10.1029/2008GL037079.

Hurrell, J. W., J. J. Hack, D. Shea, J. M. Caron, and J. Rosinski (2008), A new sea surface temperature and sea ice boundary dataset for the Community Atmosphere Model, *J. Clim.*, *21*, 5145–5153.

Jaiser, R., K. Dethloff, D. Handorf, A. Rinke, and J. Cohen (2012), Impact of sea ice cover changes on the Northern Hemisphere atmospheric winter circulation, *Tellus A*, *64*, 11595, doi:10.3402/tellusa.v64i0.11595.

Jaiser, R., T. Nakamura, D. Handorf, K. Dethloff, J. Ukita, and K. Yamazaki (2016), Atmospheric autumn and winter response to Arctic sea ice changes in reanalysis data and model simulations, *J. Geophys. Res. Atmos.*, *121*, 7564–7577, doi:10.1002/2015JD024679.

Kidston, J., A. A. Scaife, C. Hardiman, D. M. Mitchell, N. Butchart, M. P. Baldwin, and L. J. Gray (2015), Stratospheric influence on tropospheric jet streams, storm tracks and surface weather, *Nat. Geosci.*, *8*, 433–440.

Kim, B. M., S. W. Son, S. K. Min, J. H. Jeong, S. J. Kim, Z. Zhang, T. Shim, and J. H. Yoon (2014), Weakening of the stratospheric polar vortex by Arctic sea-ice loss, *Nat. Commun.*, *5*, 4646.

Kimoto, M., F.-F. Jin, M. Watanabe, and N. Yasutomi (2001), Zonal-eddy coupling and a neutral mode theory for the Arctic Oscillation, *Geophys. Res. Lett.*, *28*, 737–740, doi:10.1029/2000GL012377.

King, M. P., M. Hell, and N. Keenlyside (2015), Investigation of the atmospheric mechanisms related to the autumn sea ice and winter circulation link in the Northern Hemisphere, *Clim. Dyn.*, doi:10.1007/s00382-015-2639-5.

Limpasuvan, V., and D. L. Hartmann (2000), Wave-maintained annular modes of climate variability, *J. Clim.*, *13*, 4414–4429.

Liu, J.-P., J. A. Curry, H. Wang, M. Song, and R. M. Horton (2012), Impact of declining Arctic sea ice on winter snowfall, *Proc. Natl. Acad. Sci. U.S.A.*, *109*, 4074–4079, doi:10.1073/pnas.1114910109.

Mori, M., M. Watanabe, H. Shiogama, J. Inoue, and M. Kimoto (2014), Robust Arctic sea-ice influence on the frequent Eurasian cold winters in past decades, *Nat. Geosci.*, *7*, 869–873.

Nakamura, T., K. Yamazaki, K. Iwamoto, M. Honda, Y. Miyoshi, Y. Ogawa, and J. Ukita (2015), A negative phase shift of the winter AO/NAO due to the recent Arctic sea-ice reduction in late autumn, *J. Geophys. Res. Atmos.*, *120*, 3209–3227, doi:10.1002/2014JA020764.

Nakamura, T., K. Yamazaki, K. Iwamoto, M. Honda, Y. Miyoshi, Y. Ogawa, Y. Tomikawa, and J. Ukita (2016), The stratospheric pathway for Arctic impacts on midlatitude climate, *Geophys. Res. Lett.*, *43*, 3494–3501, doi:10.1002/2016GL068330.

Petoukhov, V., and V. A. Semenov (2010), A link between reduced Barents-Kara Sea ice and cold winter extremes over northern continents, *J. Geophys. Res.*, *115*, D21111, doi:10.1029/2009JD013568.

Screen, J. A., and I. Simmonds (2013), Exploring links between Arctic amplification and mid-latitude weather, *Geophys. Res. Lett.*, *40*, 959–964, doi:10.1002/grl.50174.

Screen, J. A., I. Simmonds, C. Deser, and R. Tomas (2013), The atmospheric response to three decades of observed Arctic sea ice loss, *J. Clim.*, *26*, 1230–1248, doi:10.1175/JCLI-D-12-00063.1.

Screen, J. A., and I. Simmonds (2014), Amplified mid-latitude planetary waves favour particular regional weather extremes, *Nat. Clim. Change*, *4*, 704–709.

Semmler, T., T. Jung, and S. Serrar (2016), Fast atmospheric response to a sudden thinning of Arctic sea ice, *Clim. Dyn.*, *46*, 1015–1025, doi:10.1007/s00382-105-2629-7.

Sun, L., C. Deser, and R. A. Tomas (2015), Mechanisms of stratospheric and tropospheric circulation response to projected Arctic sea ice loss, *J. Clim.*, *28*, 7824–7845.

Thompson, D. W. J., and J. M. Wallace (1998), The Arctic Oscillation signature in the wintertime geopotential height and temperature fields, *Geophys. Res. Lett.*, *25*, 1297–1300, doi:10.1029/98GL00950.

Thompson, D. W. J., and J. M. Wallace (2001), Regional climate impacts of the Northern Hemisphere annular mode, *Science*, *293*, 85–89.

Wu, Y., and K. L. Smith (2016), Response of Northern Hemisphere midlatitude circulation to Arctic amplification in a simple atmospheric general circulation model, *J. Clim.*, *29*, 2041–2058, doi:10.1175/JCLI-D-15-0602.1.

Yang, X., X. Yuan, and M. Ting (2016), Dynamical link between the Barents-Kara Sea ice and the Arctic Oscillation, *J. Clim.*, doi:10.1175/JCLI-D-15-0669.1, in press.

Geophysical Research Letters

Supporting information for

On the atmospheric response experiment to a Blue Arctic Ocean

Tetsu Nakamura[1,2]*, Koji Yamazaki[1,2], Meiji Honda[3], Jinro Ukita[3], Ralf Jaiser[4], Dörthe Handorf[4], and Klaus Dethloff[4]

[1] Faculty of Environmental Earth Science, Hokkaido University, Sapporo, Japan
[2] Arctic Environmental Research Center, National Institute of Polar Research, Tokyo, Japan
[3] Faculty of Science, Niigata University, Niigata, Japan
[4] Helmholtz-Zentrum für Polar- und Meeresforschung, Alfred-Wegener-Institut, Potsdam, Germany

*Corresponding author: T. Nakamura (nakamura.tetsu@ees.hokudai.ac.jp)

Contents of this file

S1. Sea ice distributions prescribed in the experiments and corresponding turbulent heat flux anomalies and geopotential height patterns

Distributions of the sea ice thickness (SIT) prescribed as the boundary condition of our model are shown for August-September-October (ASO) and November-December-January (NDJ) seasons in Figures S1a and S1b, respectively. Because the present-day sea ice reduction over the Arctic is reflected in *AICE* case, the winter sea ice anomaly and corresponding turbulent heat flux anomaly concentrate in the Atlantic side of the Arctic Ocean (Figure S1c, *AICE*). On the other hand, the sea ice is reduced artificially and impartially over the Arctic in *Im30* and *Im40* cases. Therefore, sea ice and heat flux anomalies are also found in the Pacific

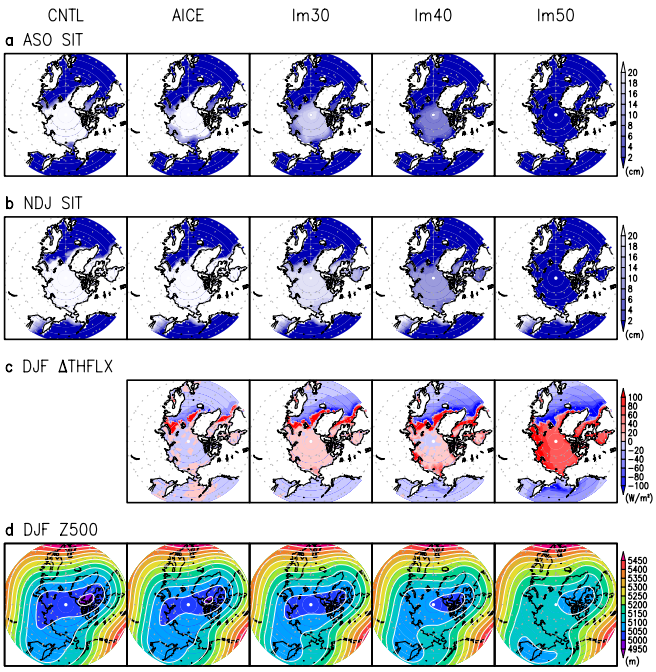

Figure S1. a, August-September-October averaged sea ice thickness (SIT) prescribed in the respective runs. **b,** Same as **a** but for November-December-January average. **c,** December-January-February averaged turbulent heat flux anomaly of the respective runs. Anomaly is defined as difference of 150-year averages between the respective runs and *CNTL* run. Red (blue) color indicates positive anomaly corresponding to the upward (downward) heat flux. **d,** December-January-February averaged 500 hPa geopotential height averaged over 150-year period of the respective runs.

side, i.e., the East Siberian Sea, the Chukchi Sea, and the Beaufort Sea (Figure S1c, *Im30* and *Im40*). Furthermore, in *Im50* case there is no sea ice all over the Arctic Ocean. This induces that the heat flux anomaly is the largest and extending to the North Pole region (Figure S1c, *Im50*). As a result, minimum of the geopotential height is not seen over the Arctic (Figure S1d, *Im50*).

S2. Estimation of heating rate anomaly due to the anomalous residual mean circulation changes

We estimated the heating rate associated with the residual mean vertical motion (w^*) obtained from our TEM analysis. Following explanation is a quotation from Appendix B of Nakamura et al. (2015) with slight changes according to this study. First, we calculate potential temperature advection due to the vertical motion, as follows:

$$\left[\frac{\partial\theta}{\partial t}\right] = -(w^*)'\frac{\partial\bar{\theta}}{\partial z^*} \tag{1}$$

where θ is potential temperature, w^* is the residual mean vertical velocity, $z^* = -H\log(p/p_0)$ (where H is the scale height (assumed to be 7 km), p and p_0 are the pressures at a given level and the surface pressure (1000 hPa), respectively), $()'$ indicates an anomaly of respective runs and an overbar indicates the climatology, which are defined as 150-year averages of *CNTL* run.

We obtain the heating rate per unit mass as follows

$$Q^* = Cp(p/p_0)^{\kappa}\left[\frac{\partial\theta}{\partial t}\right] \tag{2}$$

where Cp is the specific heat at constant pressure and κ is the Poisson constant. Finally, for comparison with the turbulent heat flux due to ice reduction, we obtain the heating rate per unit area from vertical integration of Q^* between 850 and 300 hPa:

$$J = \frac{1}{g}\int_{p=850hPa}^{p=300hPa} Q^*\,dp \tag{3}$$

where g is gravitational acceleration; thus, J indicates the dynamical heating rate over the free troposphere.

S3. Planetary-scale wave responses in the lower stratosphere

To examine the planetary-scale wave responses in the lower stratosphere, we compare the January geopotential height anomalies at 100 hPa (ΔZ100, Figure S3a). The positive height anomalies corresponding to the negative AO-like pattern are commonly found in all cases. On the other hand, the clear difference is found in the eastern Siberia where the negative anomaly in *AICE* case and positive anomaly in *Im50* case are contrast. An intensity of the climatological Siberian trough in the lower stratosphere mainly determines the upward propagation of the planetary-scale wave into the stratosphere (Nakamura et al., 2016). Then, we decomposed the climatological and anomalous geopotential height pattern into wave-1 and wave-2 component

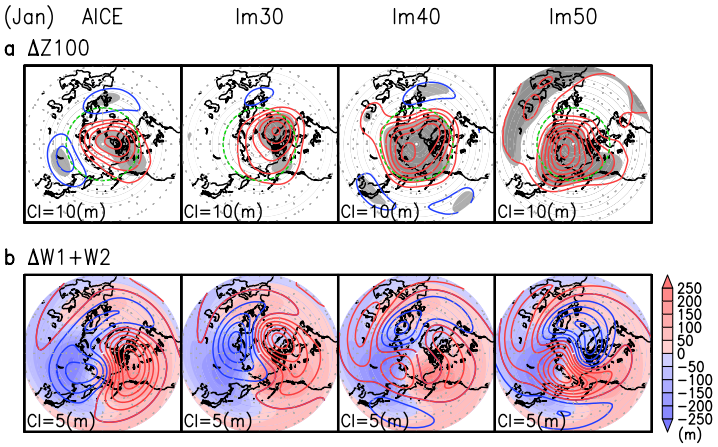

Figure S3. a, January 100 hPa geopotential height anomalies of the respective runs minus *CNTL* run. Corresponding run name is designated at the top of the panel. Contour interval is displayed at the bottom-left corner of the panel. Light and heavy grey shades indicate statistical significance greater than 95% and 99%, respectively. Green dashed line indicates a latitude circle of 60°N. **b,** As in **a** but for wave-1 plus wave-2 component of anomalies (contours) and climatology (shading). Climatology is defined as 150-year average of *CNTL* run.

(Figure S3b). It clearly shows contrast between the intensified Siberian trough in *AICE* case and weakened in *Im50*, and *Im30* and *Im40* cases are intermediate between them. The difference is likely due to the anomalous heat source associated with sea ice reduction in the Pacific side of the Arctic Ocean, which causes positive height anomalies only in *Im30* to *Im50* cases. Such the planetary-scale wave response and its impact on the stratospheric polar vortex intensity are quite consistent with Sun et al. (2015).

S4. Planetary-scale wave responses in the troposphere

We here compare the November-to-March averaged tropospheric signals in *AICE* and *Im50* cases. In *AICE* case the positive turbulent heat flux anomaly is found only in the Atlantic side of the Arctic Ocean (Figure S4a). In association with this heat flux, positive anomaly of geopotential height at 500 hPa (Z500) appears over there, and it is accompanied by the negative anomaly of Z500 over the eastern Siberia. According to the anomalous Z500 pattern upward planetary-scale wave activity (i.e., eddy heat flux, v'T') intensifies over the Siberia (Figure S4b). This feature is quite close to the tropospheric stationary Rossby wave response to the Arctic sea ice reduction (Honda et al., 2009), which induces the negative phase shift of the AO polarity (Nakamura et al., 2015). In *Im50* case the positive turbulent heat flux anomaly extends to the whole Arctic Ocean, and thus Arctic positive Z500 anomaly and Siberian negative anomaly move eastward. The positive Z500 anomaly over the East Siberian Sea connects with Z100 anomaly, which weakens climatological planetary-scale wave in the lower stratosphere as shown in Supplementary S3. In the troposphere, however, the corresponding planetary-scale wave activity over the Siberia intensifies similar to *AICE* case.

In both cases, due to the stationary Rossby wave response, the tropospheric planetary-scale wave activity intensifies in the mid-latitude (Figure S4c), comparable with that in the high-latitude. This directly induces the negative AO-like response independent with the stratospheric process as presented in the previous study (Nakamura et al., 2015). Further discussion about the independency between the stratospheric and tropospheric processes in terms of the planetary-scale wave forcing will be done in the next section S5.

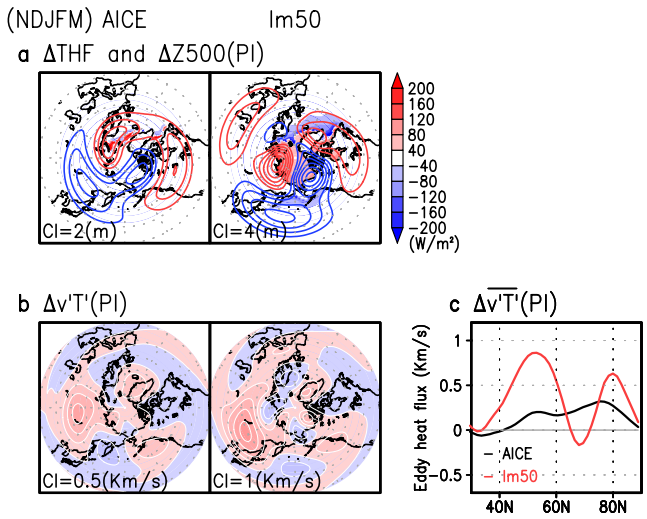

Figure S4. a, November-to-March averaged anomalies of (shading) turbulent heat flux and (contour) W1+W2 component of geopotential height at 500 hPa. Contour interval is displayed at the bottom-left corner of the panel. **b,** Eddy heat flux anomaly (Δv'T') due to W1+W2 component. **c,** Corresponding zonal mean eddy heat flux anomalies.

S5. Different control level of the wave forcing due to upward wave activity

While the tropospheric planetary-scale wave activity intensifies both in *AICE* and *Im50* cases (Figure S4b), the lower stratospheric wave activity strengthens in *AICE* but unchanges in *Im50* (Figure 2c). This is reasonable because the tropospheric and the lower stratospheric wave activities are not necessarily directly connecting with each other. Using ERA-interim data, we examined that variation of the winter stratospheric zonal wind at 60N 10 hPa is well correlated with preceding Fz anomaly above the lower stratosphere but not correlated with the Fz in the troposphere (Fig. S5. top-left panel). On the other hand, variation of the winter tropospheric zonal wind at 60N 300 hPa is well correlated with preceding Fz anomaly in the mid-latitude troposphere (Fig. S5. top-right panel). Such the different control level of the wave forcing is well represented in AFES simulation (Fig. S5. bottom panels). From this, it is strongly suggested that the lower stratospheric planetary-scale wave structure depending on the location of the surface heat flux anomaly is a controlling factor of the stratospheric polar vortex intensity rather than the tropospheric planetary-scale wave response.

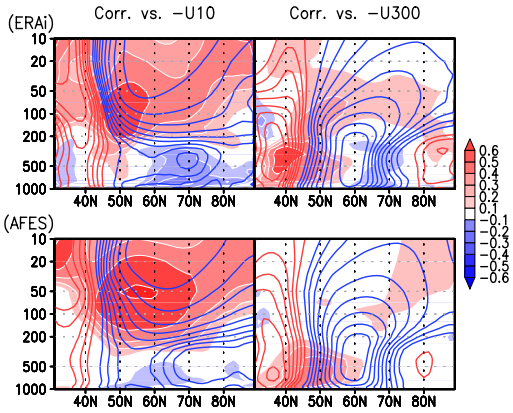

Figure S5. Shading indicates correlation coefficients between December-January mean Fz due to Wave1+2 and sign-reversed time series of January-February mean zonal mean zonal wind at 60N and at (left) 10 hPa and (right) 300 hPa. Contour indicates same but for January-February mean zonal mean zonal wind. Contour interval is 0.1 without zero line. (top) 36 years of 1979-2014 period of ERA interim data are used. (bottom) 150 years of AFES *CNTL* run data are used.

S6. Residual mean circulation responses to the Arctic sea ice reduction

November-to-March averaged residual mean circulation responses show positive anomalies of the mass stream function in all cases (Figure S6). These anomalous secondary circulations are induced by the upper tropospheric wave forcing to balance the zonal momentum (e.g., Hynes et al., 1991). Furthermore, in association with the anomalous subsidence over the Arctic and anomalous upwelling over the mid-latitudes, this anomalous circulation induces atmospheric heat transport into the Arctic.

We compared the anomalous heating rate (Figure 3c). There are significant differences in amplitudes among cases. While the turbulent heat flux nearly linearly increases with magnitudes from 1 W m^{-2} in *AICE* to 10 W m^{-2} in *Im50*, the atmospheric heat transport is comparable with magnitudes about 1 W m^{-2} between *AICE* through *Im40* and is enormously large about 5 W m^{-2} in *Im50*. This might be because of different anomalous circulation near the surface around the North Pole, that is, anomalous upwelling appears along the Arctic coast except for *Im50* case (see around 80°N 1000hPa in Figure S6). This is due to geographical difference of the surface heat source that is constantly positive all over the Arctic Ocean in *Im50* case but is positive only the coastal region of Arctic Ocean in the other cases (Supplementary Figure S1c).

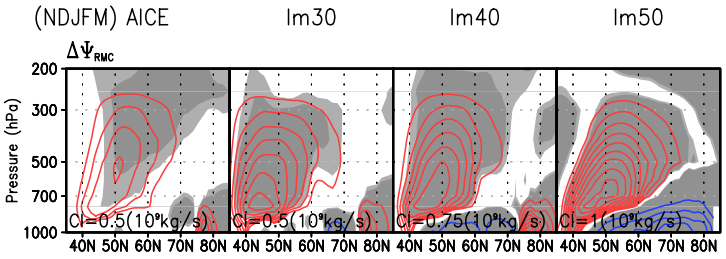

Figure S6. November-to-March averaged anomalies of mass stream function of the residual mean circulation (10^9 kg s^{-1}). Contours indicate amplitudes of the anomaly with the zero line omitted. Contour interval is displayed at the bottom-left corner of the panel. Positive anomaly indicates anomalous ascending in the lower latitudes and descending in the higher latitudes, and negative anomaly vice versa. Note that contour intervals of the negative anomalies are magnified by a factor of 10 to avoid jammed contours near the surface where TEM diagnosis is no longer reliable. Light and heavy grey shadings indicate statistical significance over 95% and 99%, respectively.